NJC

Accepted Manuscript

This is an *Accepted Manuscript*, which has been through the Royal Society of Chemistry peer review process and has been accepted for publication.

Accepted Manuscripts are published online shortly after acceptance, before technical editing, formatting and proof reading. Using this free service, authors can make their results available to the community, in citable form, before we publish the edited article. We will replace this *Accepted Manuscript* with the edited and formatted *Advance Article* as soon as it is available.

You can find more information about *Accepted Manuscripts* in the Information for Authors.

Please note that technical editing may introduce minor changes to the text and/or graphics, which may alter content. The journal's standard Terms & Conditions and the Ethical guidelines still apply. In no event shall the Royal Society of Chemistry be held responsible for any errors or omissions in this *Accepted Manuscript* or any consequences arising from the use of any information it contains.

ROYAL SOCIETY OF CHEMISTRY

www.rsc.org/njc

Precursor driven selective synthesis of hexagonal chalcocite (Cu_2S) nanocrystals : Structural, optical, electrical and photo catalytic properties

Gopinath Mondal[a], Pradip Bera[a], Ananyakumari Santra[a], Sumanta Jana[b], Taraknath Mondal[c], Anup Mondal[b], Sang Il Seok[c,d] and Pulakesh Bera[a]*

[a]*Post Graduate Department of Chemistry, Panskura Banamali College, Vidyasagar University, Midnapore (E), West Bengal-721152, India*

[b]*Department of Chemistry, Indian Institute of Engineering Science and Technology (IIEST),Shibpur, West Bengal-711103, India*

[c]*KRICT-EPFL Global Research Laboratory, Division of Advanced Materials, Korea Research Institute of Chemical Technology, 141 Gajeong-Ro, Yuseong-Gu, Daejeon 305-600, South Korea*

[c]*Department of Energy Science, Sungkyunkwan University, Suwon 440-746, South Korea*

Abstract

The reaction of $CuCl_2$, $2H_2O$ with methyl ester of 3,5-dimethyl pyrazole-1-dithioic acid (**mdpa**) yields blackish brown complex of composition, $[Cu(mdpa)_2][CuCl_2]$. The complex formed well-defined crystal and is characterized by single-crystal X-ray diffraction, thermogravimetry (TG), and spectroscopic studies. The molecule possesses a distorted tetrahedral configuration with CuN_2S_2 chromophore with +1 oxidation state of copper. TG study reveals that the molecule is a suitable precursor for copper sulfide nanoparticles. The low temperature thermal decomposition of the single-source precursor produces hexagonal chalcocite (Cu_2S) nanostructures in ethylene diamine and ethylene glycol. Selective synthesis of copper rich high chalcocite was obtained using the new precursor. The size and morphology of the synthesized Cu_2S nanoparticles are guided by the precursor and likely to be less dependent on the solvent used in the experiment. The nanoparticles were characterized by X-ray diffraction, scanning electronic microscope, and

UV-Vis spectroscopic studies. The optical band gap of the as-synthesized Cu_2S nanoparticles is measured to be 1.80 – 2.40 eV. The Cu_2S nanoparticles are found to be good catalysts in UV photo catalytic decomposition (90%) of Congo red (CR) dye following first order reaction kinetics and the reusability study of the Cu_2S catalyst also shows excellent catalytic performance (80%).

1. Introduction

Recently, the development of single-source molecular precursor for the preparation of binary and ternary semiconductor nanocrystals (NCs) has been attracted considerable attention as single-source precursor (SP) route provides special key advantages over the other conventional methods for preparing inorganic powders, nanoparticles, and thin films. Firstly, the single-source precursors can be obtained easily in ambient conditions. These are mostly metal-organic or organo-metallic compounds which have century long advanced science. Secondly, the protocol of single-source route is based on the advantages of mildness, safety and simplified one-pot synthesis of NCs.[1–3] Lastly, the presence of all constituent elements in required atomic ratios is chemically maintained in a SP strategy, which offers a clean synthetic method to produce pure compounds. The ease of synthesis of single-source precursors in ambient conditions popularizes the use of it in preparation of semiconductor chalcogenides.

Copper sulfide (Cu_xS where x= 1 to 2) is one of the chalcogenides that has received considerable attention in recent years owing to wide stoichiometric compositions, nanocrystals morphologies, hierarchical structure. The stoichiometric composition of copper sulfide varies from copper rich Cu_2S to copper deficient CuS_2 such as Cu_2S, $Cu_{1.96}S$, $Cu_{1.94}S$, $Cu_{1.8}S$, $Cu_{1.75}S$, and CuS with varying morphology[4] and different unique optoelectronics properties.[5–7] The bandgap of copper sulfide can vary in a wider range (1.2 to 2.5 eV) with stoichiometric composition, which makes it

a highly desirable material for solar cells,[8,9] nonvolatile memory devices,[10] nano-scale switches, [11] lithium ion batteries,[12] gas sensing [13,14] and theranostic applications. [14]

In literature, various SP have been used for the synthesis of copper sulfide nanoparticles with different shapes and sizes and morphologies. For instance, Liu et al.[15] decomposed $Cu(S_2CNEt_2)_2$ in a mixture of dodecanethiol and oleic acid to obtained wires of hexagonal Cu_2S (chalcocite), while Lou et al.[16] decomposed $Cu(S_2CNEt_2)_2$ in TOP/TOPO to obtain spherical $Cu_{1.8}S$ (digenite) nanocrystals. Corncoblike Cu_2S nanostructures were obtained through thermolysis of copper dithiolate in dodecanethiol.[17] Korgel et al. prepared Cu_2S nanorods, nanodisks, and nanoplatelets by solventless thermolysis of a copper-alkylthiolato precursor.[18] In a report, Li et al. synthesized of monodispersed Cu_2S nanocrystals by the reaction of Cu(II)-stearate and dodecanethiol in 1-octadecene.[19] Hydrothermal growth of CuS nanowires from Cu-dithiooxamide was reported by Roy and Srivastava.[20] Almost all of the reported SP methods have been performed using hazardous external surfactants. Various factors such as nature and concentration both of the precursor and capping agent have an influence in the rate of nucleation and growth, and hence the morphology of particles.[21–24] Very recently, Liberto Manna group reported the use of Cu(I) complex, $[Cu(CH_3CN)_4]PF_6$, to prepare platelet-shape copper sulfide nanocrystals from covellite ($Cu_{1.1}S$) where Cu : S ratio could be gradually increased from 1.1 : 1 to 2 : 1 retaining their overall size and morphology.[25] The same Cu(I) complex was also used by the same group to increase in Cu content of $Cu_{2-x}Se$ NCs.[26] In each case, the Cu(I) complex, $[Cu(CH_3CN)_4]PF_6$, helps to form copper rich copper sulfide NCs but the mechanism is unclear to them. In a another report, Nair and Scholes concluded that the SP derived from thiosemicarbazide, a NS chelate, are generally effective in evaluating anisotropic structure of the NCs where the ligand internally acts as structure directing agent.[27] The use of functional

molecules as capping ligands in SP to control the shape, size, and also the assembly structure of nanocrystallites in the solution-phase synthesis has been extensively studied. So the rational design and synthesis of ligands is very crucial for the preparation of SP that could be used to prepare hierarchical structure of particles through SP route. Moreover, the oxidation state of metal in SP has also great influence to the final product. In literature, the SP route to synthesize copper rich Cu_2S or copper deficient CuS in presence of reducing agent(s) with varying morphologies and stoichiometries were obtained using mainly the metal–organic compounds of Cu(II).[1–3, 21–24] The reduction of Cu(II) to Cu(I) is required to form copper rich morphologies e.g., $Cu_{1.8}S$, $Cu_{1.96}S$, Cu_2S etc and most of the cases the reducing agents/solvents were used to reduce the Cu(II) species to Cu(I). The effort to synthesize the funtionalized SP where the oxidation state of copper is chemically maintained to +1 is practically rare. Consequently, the use of Cu(I) complex is also limited to prepare copper rich copper sulfide NCs. We report the synthesis of a new SP of heterocyclic NS-chelate where the oxidation state of copper in the SP is chemically maintained to +1. Further the SP is used in selective preparation of copper rich Cu_2S NCs without using any reducing agent.

In search of NS-chelates having ability to direct of particles morphology for NCs, we synthesize a new pyrazolyl ligand **mdpa** and its copper(I) complex, $[Cu(mdpa)_2][CuCl_2]$. Pyrazolyl compounds are being considered as ancillary ligands due to their fascinating mode of coordination which is reflected in literature and text books of chemistry. Pyrazole (1, 2 diazole) is isomeric with imidazole (1, 3 diazoles) which are commonly found in biologically active compounds such as natural products, protein ligands and pharmaceuticals. The structural unit of pyrazole is rarely found in nature but serves as important core structures of many pharmaceuticals with wide range of biological activities such as cholesterol lowering,[28] anti-

inflammatory,[29] anticancer,[30] antidepressant, and antipsychotic agents.[31] As a result, there is a continuing interest in the development of versatile methods to access highly substituted pyrazoles. Here we report, (i) the synthesis of pyrazolyl ligand (mdpa) and its Cu(I) complex, (ii) the use of the new Cu(I)-complex to selective preparation of Cu_2S NCs, and (iii) the as-synthesized Cu_2S particles were used as catalyst in photo degradation of Congo red (CR).

2. Experimental details

2.1 Chemicals

Copper chloride, carbon disulfide (Merck), methyl iodide (Spectrochem), ethylene diamine (Himedia), and ethylene glycol (Himedia), were all of analytical grade and used without further purification. Solvent ethanol (Changshu Yangyuan Chemical, China) was dried and distilled before use.

2.2 Synthesis of methyl ester of 3,5-dimethyl pyrazole-1-carbodithioc acid (mdpc) and [Cu(mdpc)$_2$][CuCl$_2$]

Carbon disulfide (0.99 g, 13 mmol) was added in a small portion to a mixture of 3,5-dimethylpyrazole (0.97 g, 10.0 mmol) in tetrahydrofuran (15 mL) and finely powder KOH (0.58 g, 10.3 mmol) in room temperature with constant stirring. The solution turned yellow to orange where a heavy mass of 3,5-dimethyl pyrazole-1-carbodithioc acid (dpc) separated out which was immediately filtered and thoroughly washed with diethyl ether and dried in vacuo over P_4O_{10}. 3.18 g (15 mmol) of properly dried dpc was dissolved in 50 mL of distilled water in a 250 mL round bottom flask placed in an ice-bath (0 °C). Methyl iodide (1 mmol, 2.12 g) was added slowly and drop wise for the period of 30 minutes to an aqueous solution (50 mL) of dpc (3.18 g,

15 mmol) with constant stirring. The stirring was continuing for additional 1 hr where a yellow colour compound of methyl ester of 3,5-dimethyl pyrazole-1-carbodithioc acid (mdpa) was separated out, filter off, washed with water and dried over silica gel. Yield: 82%. M.P. (decomposed): 30 °C. Anal. Calc. for $C_7H_{10}N_2S_2$: C, 45.13; H, 5.41; N, 15.04; S, 34.42. Observed: C, 45.01; H, 5.72; N, 15.48; S, 33.88. IR (cm^{-1}): 3398-3476, υ(O-H); 980, υ(C=S); 1575, υ(C=N); 1490, υ(C-N).

$CuCl_2$. $2H_2O$ (10 mmol, 1.70 g) dissolved in 20 mL of ethanol was added drop wise to an ethanolic solution of mdpa (10 mmol, 1.86 g) dissolved in 20 mL ethanol with constant stirring. Stirring is continued for another half an hour where a deep blue colour compound separated out. The precipitate formed was filtered, washed with excess ethanol and dried in an oven at 90 °C. Yield: 80%, Mass spectrum m/z value: 435.10 (molecular ion peak). Anal. Calc. for $C_{14}H_{20}C_{l2}N_4S_4Cu_2$: C, 29.47; H, 3.53; N, 9.82; S, 22.48%. Observed: C, 29.46; H, 3.05; N, 9.70; S, 22.78%. The chemical reaction for the preparation of the precursor is detailed in Scheme 1.

2.3 Preparation of copper sulfide nanoparticles using $[Cu(mdpa)_2][CuCl_2]$

In a solvothermal synthesis, 0.285 g (0.5 mmol) of as prepared precursor, $[Cu(mdpa)_2][CuCl_2]$, was taken with 15 mL of solvent in a 50 mL two-necked round bottom flask equipped with a condenser and thermocouple adaptor. The flask was degassed at room temperature for 5 minutes and then filled with inert nitrogen gas. The resulting solution was then gradually heated to 150 °C and maintained the reaction temperature for 30 minutes. The same set of experiments was also done at 180 °C for 1 h. The black precipitate formed was collected through centrifugation and washed 4 to 5 times with ethanol. Dry powder of copper sulfide NCs were collected by evaporating ethanol at 100 °C for 1 hr. in oven.

2.4. Characterization

The single crystal X-ray diffraction was carried out on a Bruker SMART APEX II X-ray diffractometer equipped with graphite-monochromated Mo-Kα radiation (λ = 0.71073 Å) and 16 CCD area detector. The intensity data were collected in the π and ω scan mode, operating at 50 kV, 30 mA at 296 K.[32] The data reduction was performed using the SAINT and SADABS programs.[33] All calculations in the structural solution and refinement were performed using the Bruker SHELXTL program.[34] The structure was solved by the heavy atom method and refined by full-matrix least-squares methods. All the non-hydrogen atoms were refined anisotropically; the hydrogen atoms were geometrically positioned and fixed with isotropic thermal parameters. The final electron density maps showed no significant difference. Mass spectra of both ligand and metal complex were obtained using a Waters HRMS XEVO-G2QTOF#YCA351. The elemental analysis (C, H, N, and S) of the complex was performed using FISONS EA-1108 CHN analyzer. The IR spectra ($4000cm^{-1}$–$500cm^{-1}$) were recorded on a Perkin Elmer Spectrum Two FT-IR Spectrophotometer with sample prepare as KBr pellets. TG analysis was carried out on a TGA NETZSCH TG 209 F1 instrument at a heating rate of 10 ^{o}C/min under nitrogen. UV-Visible absorption spectra of the samples were recorded on a Perkin Elmer Lambda 35 spectrophotometer in the wavelength range region 200–800 nm at room temperature. Powder X-ray diffraction (XRD) of the NCs was recorded using a Seifert XDAL 3000 diffractometer using graphite-monochromated Cu–Kα radiation (λ = 1.5418 Å) with a scan rate 5°/min over a range of $5°<2\theta < 80°$ with steps of 0.02° and scintillation detector is operating at 40 kV and 40 mA. TEM and HRTEM of copper sulfide NPs were characterized using a FEI Tecnai G2 T-20S at an accelerating voltage 200kV. The TEM samples were prepared by placing a drop of a dilute ethanol dispersion of NCs on the surface of a 200-mesh carbon-coated copper grid. The SEM

and FESEM of NCs were analyzed with a Gemini Zeiss Supra 40VP (Carl Zeiss Micro imaging GmbH, Berlin, Germany) field emission scanning electron microscope (FESEM) with 20 kV accelerating voltage. Energy dispersive X–ray (EDX) analysis of the sample was carried out on Oxford instrument INCA attached to the SEM in the scanning range of 20 keV. Photocatalytic activity of Cu_2S was studied with a 50 mL of 0.5×10^{-3} M aqueous solution of CR in a 100 mL beaker using visible light source. A 250 W indoor fluorescent lamp was used as light source. To test the photocatalytic degradation of CR, a solution of known CR concentration and Cu_2S NCs photocatalyst was allowed getting adsorption equilibrium for 120 min in the darkness. Then the solution was exposed to visible light irradiation under magnetic stirring. At 15 min interval, 3.5 mL of suspension was sampled and centrifuged to remove the photocatalyst powders. The concentration of the dye after photocatalyst degradation was determined with a UV-Vis spectrophotometer.

3. Result and Discussions

3.1 Synthesis and characterization of SP with X-ray crystallographic study

The selective synthesis of Cu_2S morphology could be possible with an internally active Cu(I)-precursor in single-source solvothermal route. In search of new Cu(I) SP, the N-heterocycle based ligands like pyrazole, imidazole, pyrimidine etc. are chosen because of their special ability to stabilize the lower oxidation states of metal due to their π-acidity.[35] Pyrazoles can be used as ligand or as precursors of pyrazole-based ligands and are accessible by well-established synthetic methods.[35] These methods are quite general and this allows the preparation of pyrazoles with a variety of substitution patterns and with different functionalities as substituent

of the pyrazole ring. Pyrazole having two equivalent N-atoms with localized lone pair (σ-donor) on an in-plane orbital and vacant low lying anti bonding π* orbitals (perpendicular to the molecular plane) shows versatile bonding capabilities with metal ions and there has been a growing interest in new synthetic methods for the preparation of pyrazole derived ligands and their metal complexes. A pyrazole based dithiocarbazate is used to develop a new internally functionalized single source precursor for copper sulfide nanocrystals. The ligand mdpa and the copper complex were isolated from ethanol in very good yields. It is interesting to note that solid state isolation of Cu(I) complex is possible starting with a Cu(II) salt i.e., cupric chloride. The sulfur containing pyrazolyl ligand mdpa reduces Cu(II) to Cu(I) at the same time stabilizes lower oxidation state of copper in the reaction condition.[36] The compounds are microcrystalline, stable in air soluble in some organic solvents.

The Fig.1 shows the FTIR spectra of the free ligand and the copper complex. In order to confirm the mode of bonding of the ligand, the FTIR spectra of the free ligand and the copper complex were studied and assigned on careful comparison of metal complexes with that of free ligand. The peaks in the spectrum of complex are less in number and quite sharp than that of ligand spectrum clearly proves the strong bonding of ligand(s) with metal. A very broad band typical of water in the 3476–3398 cm^{-1} region is a proof of hygroscopic nature of the ligand. The ligand shows the bands assigned to υ(C=N) and υ(C–N) at 1586 cm^{-1} and 1324 cm^{-1} respectively. An increase in υ(C–N) in the free ligand spectrum by *ca.* $\Delta\upsilon = 7$ cm^{-1} on complex formation [υ(C–N) =1331 cm^{-1} in complex], as well as increase ($\Delta\upsilon = 55$ cm^{-1}) in υ(C=N) indicate a coordination through tertiary pyrazole ring nitrogen atom. The coordination of thione sulfur atom to metal centre is indicated by a decrease of the υ(C=S) band from 980 cm^{-1} (in free ligand) to 913 cm^{-1} in its complex.

TG analysis of the complex is conducted to study the thermal behavior and suitability for the preparation of CuS NCs. The decomposition of the complex started near 100 °C as shown in Fig. 2. The complex undergoes significant weight loss of 33% (*ca.* 33.21%) in first stage between temperatures 100 °C to 200 °C due to the loss of fragment A along with one Cl. The same loss of units (A) and Cl is repeated over a temperatures range 200 °C to 700 °C in the second stage of decomposition giving a residue, which is close to the value calculated for the mass percentage of bulk CuS (33.38%). The decomposition steps are shown in the Scheme – 2.

The molecular structure of SP, $[Cu(mdpa)_2][CuCl_2]$, has been established by X-ray crystallography. The ORTEP diagram with atom numbering scheme is shown in Fig. 3. The crystallographic and experimental data for SP are given in Table 1 and the selected bond lengths and angles are given Table 2. The coordination geometry around the Cu-atom is tetrahedral with an N_2S_2 chromophore with the participation of two ligand moieties. Cu(I) is coordinated by the ternary N-atom and thione sulfur of each ligand and $CuCl_2$ unit is present outside the coordination sphere to satisfy the residual charge. In the complex, the chelate bite angle of N(2) –Cu(1)–S(1) and N(12)–Cu(1)–S(11) are 84.52(7)° and 84.39(7)°, respectively. These angles are much smaller than the ideal tetrahedral angle (109.28°) as well as the other two tetrahedral angles N(2)–Cu(1)–N(12) [108.3(10)°] and S(1)–Cu(1)–S(11) [121.61(3)°]. The lowering of the biting angles is due to the closeness of the coordinating N and S atoms in the ligand with a view to facilitate the formation of 5–membered chelate rings. The biting angle N(2)–Cu(1)–N(12) [108.3(10)°] reveals that the out plane position of the two adjacent pyrazole rings giving less steric crowding among methyl groups at 3(5) position. Thus the distorted tetrahedral complex becomes vulnerable to ligand substitution prior to formation of nanoparticle.

3.2 Formation and characterization of Cu_2S NCs

Reaction below the decomposition temperature of the SP (*ca.* 100 °C) leads to an incomplete dissociation of the intermediate species and rendered quite aggregated product. Thus a higher reaction temperature than the decomposition temperature of SP is considered with heating duration 30 minutes or 1h. The particles obtained in a certain reaction temperature with 30 minutes heating duration are microcrystalline in nature and the crystallinity improves with increasing reaction time up to 1h. It is found that only high chalcocite (Cu_2S) is the product at any reaction temperature irrespective the solvent used in the experiment. The solventless synthesis i.e., heating of the SP in a closed quartz furnace in N_2 atmosphere gives also Cu_2S NCs. So, the SP with Cu(I) in its coordination sphere has total control on the product stoichiometry of the copper sulfide NCs and further use of any reducing agent/solvent to synthesize Cu_2S from Cu(II) salts or its complexes is not essential.

The XRD patterns of the samples prepared in EN and EG at 180 °C are shown in the Fig. 4(a) and 4(b), respectively. All these patterns show four broad peaks at 37.7°, 46.5°, 48.6°, 54.4° and 55.2° originating from (102), (110), (103), (112) and (201) lattice plane, which are very close to those reported for chalcocite Cu_2S (JCPDS card 26-1116), with the p63 space group and a primitive unit cell with a = 3.961Å and c = 6.722Å.

The morphologies of the as-prepared samples were investigated by scanning and transmission electron microscopy. The morphology of the Cu_2S NCs prepared at different temperatures using different solvents was characterized by SEM and FE-SEM and presented in the Fig. 5. Fig. 5(A) and 5(B) show the SEM and FE-SEM images of the products obtained in EN at 150 °C, respectively. The morphology of Cu_2S product is found to be cluster of nanocrystals [Fig. 5(A)]. The FE-SEM image shows clusters comprising nanoplates with hexagonal morphology. The

energy dispersive X-ray (EDX) spectrum of this sample shows a 2 : 1 Cu : S atomic ratio, indicating high chalcocite phase, as shown in Fig. 6. Further increasing the synthesis temperature to 180 °C in the same solvent (EN), achieved similar Cu_2S cluster, with diameter range of 0.1μm –0.2 μm and these are found to be less compact and the formation of uniform nanoplates is prominent in the SEM [Fig. 5(C)] and FE-SEM [Fig. 5(D)] images. SEM and FE-SEM images of the Cu_2S NCs synthesized from SP in EG at 150 °C clearly shows agglomerated cluster of both spherelike nanoparticles and nanoplates with high degree of porosity. Degree of porosity and crystallinity increase when the reaction temperature increased to 180 °C as shown in the Fig. 5(G) and 5(H) and the nanoplates morphologies prominent over the nanoparticles. Therefore, the use of SP in the solvothermal synthesis of Cu_2S furnishes porous cluster consisting of hexagonal nanoplatelets irrespective the solvent used in the reaction. It is to be noted that the crystallinity and porosity increases with increasing the reaction temperature. As a result, remarkable photocatalytic activity was shown by the synthesized Cu_2S NCs. For which the experimental details are discussed later.

Fig. 7 shows the TEM and HRTEM images of the samples prepared at different reaction conditions. When EN is employed as solvent at 150 °C for 1h, the obtained copper sulfide NCs looks spherical with size 5–7 nm [Fig. 7(A)]. Fig. 7(B) shows high magnification TEM image of NCs obtained at 180 °C. Hexagonal nanoplates are found along with the elongated NCs and the size of these elongated NCs and hexagonal plates are measured to be in the range of 60–100 nm. The measured lattice spacing of 1.98 Å is well matched to the spacing between the (110) planes of chalcocite Cu_2S [Fig. 7(C)]. Further hydrothermal synthesis of Cu_2S NCs in EG, the product morphology is found to be nearly same as that obtained in EN. Nearly spherical particles are found in the product obtained at 150 °C in EG [Fig. 7(D)]. However, the low magnified TEM

image [Fig. 7(E)] clearly show primarily hexagonal nanoplates in the size range 40 – 60 nm along with a few elongated particles. The measured lattice spacing between the (110) planes of Cu_2S is 1.98 Å [Fig. 7(F)].

The optical properties were measured using UV-Vis spectrophotometry. Fig. 8 shows the plot of absorbance vs. wavelength for the Cu_2S NCs prepared in EN and EG at 180 °C. A broad peak is observed in the visible region with long trail. The band gap plots of $(\alpha h\upsilon)^2$ vs. E(=hυ) as per Tauc's equation [$(\alpha h\upsilon = k(h\upsilon\text{-}Eg)^{1/2}$] for the direct band gap are given in the inset of Fig. 8. The measure band gap is 1.8 eV for Cu_2S prepared in EN whereas it is 2.4 eV for Cu_2S prepared in EG. This result indicates that the Cu_2S NCs have a suitable band gap for photocatalytic decomposition of organic contaminants under visible light irradiation.

3.3 Photocatalytic activity study of Cu_2S NCs

It is great importance to investigate the adsorption process of organic pollutants on the catalyst surface to clarify the mechanism of photocatalytic reactions, which can facilitates their applications in contaminant destruction. To check the potentiality of the as prepared Cu_2S NCs as photocatalyst, the catalytic performance of Cu_2S NPs were examined by the photodegradation of CR fluorescence dye under the illumination of light followed by spectrophotometric monitoring. The intensity of characteristic absorption peak of CR at 495 nm is remarkably reduced in the presence of Cu_2S NCs upon visible light irradiation with time as shown in Fig. 9. Fig. 10 displays the photodegradation of CR over Cu_2S NCs as function of Ln (C_t/C_0) *vs*. irradiation time (min) under visible light illumination. For CR concentration of 0.36 mg/L, the degradation was almost completed after illumination for 135 minutes. It seemed that the Cu_2S nanoclusters act as good catalyst in the UV-potocatalytic degradation of aqueous solution of CR. The linear relationship between lnC_0/C_t and time demonstrated that the photocatalytic

degradation of CR followed a first order kinetics: $\ln C_0/C_t = kt$ where k value calculated as 14.05×10^{-3} min^{-1}. To our knowledge the degradation of CR using Cu_2S NCs was not checked earlier.

Interestingly, the reusability study of the Cu_2S nanocluster catalyst shows 80% degradation of CR as shown in Fig. 10. This proves that the presence of complex internal cavities in the flower like cluster of NCs which restricts the easy removal of absorbed impurities on the catalytic surface.

Conclusion:

A new single source precursor derived from pyrazolyl dithiocarbazate ligand has been used to synthesize selectively hexagonal Cu_2S nanoparticles. The presence of +1 oxidation state of copper is helpful to the selective synthesis of Cu_2S. The structure of the Cu(I) complex precursor was solved by single-crystal X–ray crystallography and TG analysis of the precursor was done to check the suitability of the compound for the synthesis of copper sulfide nanoparticles. The distorted shape the tetrahedral complex of Cu(I) and low decomposition temperature (100 °C) facilitate the formation of flower like hexagonal chalcocite (Cu_2S) nanostructures with sufficient porosity and crystallinity in solvothermal process. Further, the Cu_2S nanoparticles have also been used as catalyst for photodegradation of aqueous solution of Congo red (CR) with efficiency (90%) as well as the reusable catalytic efficiency of the Cu_2S is found to be 80%. Further studies on heterocyclic based precursor will explore the structure and activity relationship for the rational synthesis of other Cu^I chalcogenide/chalcogenolate nanoparticles/thin films and their photocatalylic activities.

Acknowledgements

We gratefully acknowledge the research grant from CSIR, Government of India [grant no. 1(2534)/11/EMR-II], and UGC, Government of India [F 42-280/2013(SR)]. Sang Il Seok thanks to the Global Research Laboratory (GRL) Program and the Global Frontier R&D Program on Center for Multiscale Energy System funded by the National Research Foundation under the Ministry of Education, Science and Technology of Korea, and by a grant from the KRICT 2020 Program for Future Technology of the Korea Research Institute of Chemical Technology (KRICT), Republic of Korea.

References:

1 D. Fan, M. Afzaal, M.A. Mallik, C.Q. Nguyen, P. O'Brien and P.J. Thomas, *Coord. Chem. Rev.,* 2007, **251**, 1878–1888.

2 B.I. Kharisov, O.V. Kharissova and U.O. Mendez, *J. Coord. Chem.,* 2013, **66**, 3791–3828.

3 G. Kedarnath and V.K. Jain, *Coord. Chem. Rev.,* 2013, **257**, 1409–1435.

4 J. Kundu and D. Pradhan, *New J. Chem.,* 2013, **37**, 1470–1478.

5 Y. Wu , C. Wadia , W. Ma , B. Sadtler and A. P. Alivisatos, *Nano Lett.,* 2008, **8**, 2551–2555.

6 C.H. Lai, M.Y. Lu and L.J. Chen, *J. Mater. Chem.,* 2012, **22**, 19–30.

7 Y. Xie, L. Carbone, Concetta Nobile, V. Grillo, S. D′Agostino, F.D. Sala, C. Giannini, D. Altamura, C. Oelsner, C. Kryschi and P.D. Cozzoli, *ACS Nano,* 2013, **7,** 7352–7369.

8 L. Reijnen, B. Meester, A. Goossens and J. Schoonman, *Chem. Vap. Deposition,* 2003, **9**, 15–20.

9 M. C. Lin and M. W. Lee, *Electrochem. Commun.,* 2011, **13**, 1376–1378.

10 L. Chen, Y. D. Xia, X. F. Liang, K. B. Yin, J. Yin, Z. G. Liu and Y. Chen, *Appl. Phys. Lett.,* 2007, **91,** 073511.

11 T. Sakamoto, H. Sunamura, H. Kawaura, T. Hasegawa, T. Nakayama and M. Aono, *Appl. Phys. Lett.,* 2003, **82,** 3032.

12 L. Zhao, F. Tao, Z. Quan, X. Zhou, Y. Yuan and J. Hu, *Mater. Lett.,* 2012, **68,** 28–31.

13 A. A. Sagade, R. Sharma and I. Sulaniya, *J. Appl. Phys.,* 2009, **105**, 043701.

14 S. Goel, F. Chen and W. Cai, *small,* 2014, **10,** 631–645.

15 Z. P. Liu, D. Xu, J. B. Liang, J.M. Shen, S. Y. Zhang and T. Y. Qian, *J. Phys. Chem. B,* 2005, **109,** 10699–10704.

16 W. Lou, M. Chen, X. Wang and W. Liu, *J. Phys. Chem. C,* 2007, **111,** 9658–9663.

17 X. S. Du, Z. Z. Yu, A. Dasari, J. Ma, Y. Z. Meng and Y. W. Mai, *Chem. Mater.,* 2006, **18,** 5156–5158.

18 M. B. Sigman, A. Ghezelbash, T. Hanrath, A.E. Saunders, F. Lee and B. A. Korgel, *J. Am. Chem. Soc.,* 2003, **125**, 16050–16057.

19 X. H. Li, J. X. Li, G. D. Li, D. P. Liu and J. S. Chen, *Chem. Euro. J.,* 2007, **13,** 8754–8761.

20 P. Roy and S. K. Srivastava, *Cryst. Growth and Des.,* 2006, **6**, 1921–1926.

21 T. Mandal, G. Piburn, V. Stavila, I. Rusakova, T.O. Ely, A. C. Colson and K. H. Whitmire, *Chem. Mater.,* 2011, **23,** 4158–4169.

22 Y. Lou, A. C. S. Samia, J. Cowen, K. Banger, X. Chen, H. Lee and C. Burda, *Phys. Chem. Chem. Phys*., 2003, **5**, 1091–1095.

23 S. Gorai, D. Ganguli, and S. Chaudhuri, *Crystal Growth & Design*, 2005, **5**, 875–877.

24 P. Bera, S. I. Seok, Solid State Sciences , 2012, **14**, 1126–1132.

25 Y. Xie, A. Riedinger, M. Prato, A. Casu, A. Genovese, P. Guardia, S. Sottini, C. Sangregorio, K. Miszta, S. Ghosh, T. Pellegrino and L. Manna, *J. Am. Chem. Soc.,* 2013, **135**, 17630 –17637.

26 D. Dorfs, T. Hartling, K. Miszta, N. C. Bigall, M. R. Kim, A. Genovese, A. Falqui, M. Povia, L. Manna, *J. Am. Chem. Soc.,* 2011, **133**, 11175–11180.

27 P. S. Nair and G. D. Scholes, *J. Mater. Chem.,* 2006, **16,** 467–473.

28 D. R. Sliskovic, B. D. Roth, M. W. Wilson, M. L. Hoefle and R. S. Newton, *J. Med. Chem.* 1990, **33**, 31–38.

29 T. D. Penning, J. J. Talley, S. R. Bertenshaw, J. S. Carter, P. W. Collins, S. Docter, M. J. Graneto, L. F. Lee, J. W. Malecha, J. M. Miyashiro, R. S. Rogers, D. J. Rogier, S. S. Yu, G. D. Anderson, E. G. Burton, J. N. Cogburn, S. A. Gregory, C. M. Koboldt, W. E. Perkins, K. Seibert, A. W. Veenhuizen, Y. Y. Zhang and P. C. Isakson, *J. Med. Chem*., 1997, ***40***, 1347–1365.

30 S. R. Stauffer and J. A. Katzenellenbogen, *J. Comb. Chem.,* 2000, **2**, 318– 329.

31 K. W. Moore, K. Bonner, E. A. Jones, F. Emms, P. D. Leeson, R. Marwood, S. Patel, S. Patel, M. Rowley, S. Thomas and R. W. Carling, *Bioorg. Med. Chem. Lett.*, 1999, **9**, 1285–1290.

32 Bruker, SMART (Version 5.625) Data Collection Program, Bruker AXS Inc., Madison, Wisconsin, USA, 2001.

33 Bruker, SAINT (Version 6.28a) and SADABS (Version 2.03) Data Reduction and Absorption Correction Program, Bruker AXS Inc., Madison, Wisconsin, USA, 2001.

34 G M. Sheldrick, SHELXTL (Version 6.12) Structure Analysis Program, Bruker AXS Inc., Madison, Wisconsin, USA, 2001.

35 J. Perez and L. Riera, *Eur. J, Inorg. Chem.,* 2009, 4913 – 4925.

36 T. N. Mandal, S. Roy, A. K. Barik, S. Gupta, R. J. Butcher and S. K. Kar, *Inor. Chim. Acta.,* 2009, **362,** 1315–1322.

Scheme – 1: Synthesis of ligand and SP.

Scheme – 2: Decomposition steps of SP in TG analysis.

Table – 1: Crystallographic and experimental data for SP.

Table – 2: Selected bond length (Å) and bond angles(°) for SP.

Figure – 1: FTIR spectra of Ligand (a) and SP (b).

Figure – 2: TGA (a) and derivative of TGA (b) curves for SP.

Figure –3: Coordination environment of the copper atom in the structure of SP.

Figure –4: X-ray diffraction patterns of Cu_2S NCs prepared from SP in EN (a) and in EG (b).

Figure–5: SEM (A) and FESEM (B) of Cu_2S NCs prepared at 150 °C in EN; SEM (C) and FESEM (D) of Cu_2S NCs prepared at 180 °C in EN; SEM (E) and FESEM (F) of Cu_2S NCs prepared at 150 °C in EG; SEM (G) and FESEM (H) of Cu_2S NCs prepared at 180 °C in EG.

Figure –6: EDX spectrum of sample prepared in EN at 150 °C.

Figure–7: TEM (A) of Cu_2S NCs Prepared at 150 °C in EN; TEM (B) and HRTEM (C) of Cu_2S NCs prepared at 180 °C in EN. HRTEM (D) of Cu_2S NCs Prepared at 150 °C in EG; TEM (E) and HRTEM (F) of Cu_2S NCs prepared at 180 °C in EG.

Figure –8: UV-Vis absorption spectra of samples prepared from EN (a) and EG (b).

Figure –9: Time dependant spectral changes of CR aqueous solution by Cu_2S NCs.

Figure –10: Logarithmic change in concentration of CR as a function of irradiation time.

Scheme – 1

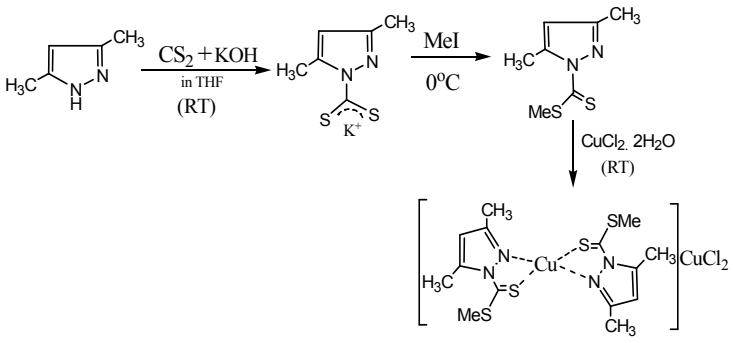

Scheme – 2

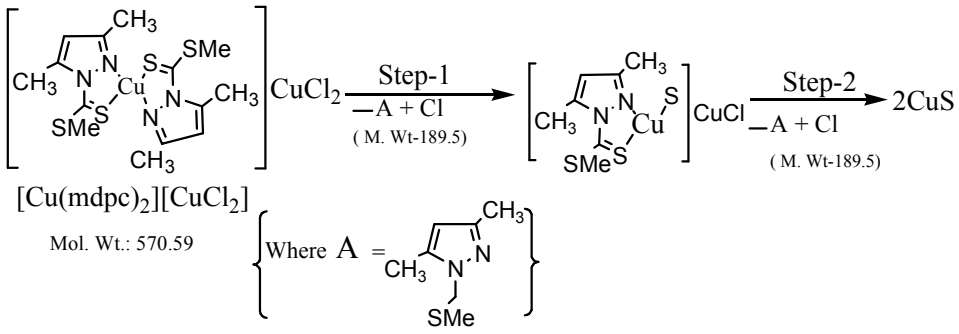

Table – 1

Empirical formula	$C_{14}H_{20}Cl_2Cu_2N_4S_4$
Formula weight	570.56
Crystal system	Triclinic
Space group	P-1
a/Å	10.5271(9) Å
b/Å	10.7784(9) Å
c/Å	10.9396(9) Å
α/°	68.855(4)°
β/°	65.795(4)°
γ/°	78.787(5)°
V/Å^3	1054.33(15)
Z	2
$D_{calc.}$/mg.m^{-3}	1.797
Absorption coefficient/mm^{-1}	2.674
F(000)	576
Reflections collected	17096
Independent reflections	5169
R(int)	0.0613
Theta(deg)	28.30°(98.6 %)
R1, wR2 [I>2σ(I)]	0.0526, 0.1342
R1, wR2 (all data)	0.0599, 0.1420
Largest diff. peak and hole/ e. Å^{-3}	1.490, -2.156

Table – 2:

Bonds	values(Å)	Bonds	values(Å)	bonds	values(Å)
C(5)-H(5A)	0.9800	C(5)-H(5B)	0.9800	C(5)-H(5C)	0.9800
C(6)-H(6A)	0.9800	C(6)-H(6B)	0.9800	C(6)-H(6C)	0.9800
S(11)-C(11)	1.666(3)	S(12)-C(11)	1.719(3)	S(12)-C(15)	1.801(3)
N(11)-C(11)	1.390(4)	N(11)-N(12)	1.396(3)	N(11)-C(12)	1.398(3)
N(12)-C(14)	1.308(4)	C(12)-C(13)	1.364(4)	C(12)-C(16)	1.489(4)
Angles	values(°)	Angles	values(°)		
N(12)-Cu(1)-N(2)	108.30(10)	N(12)-Cu(1)-S(1)	130.53(7)		
N(2)-Cu(1)-S(1)	84.52(7)	N(12)-Cu(1)-S(11)	84.39(7)		
N(2)-Cu(1)-S(11)	133.25(7)	S(1)-Cu(1)-S(11)	121.61(3)		
Cl(1)-Cu(2)-Cl(2)	175.70(4)	C(1)-S(1)-Cu(1)	99.51(10)		
C(1)-S(2)-C(5)	102.46(14)	C(1)-N(1)-N(2)	117.2(2)		
C(1)-N(1)-C(2)	132.8(2)	N(2)-N(1)-C(2)	109.9(2)		
C(4)-N(2)-N(1)	106.2(2)	C(4)-N(2)-Cu(1)	135.6(2)		
N(1)-N(2)-Cu(1)	116.89(19)	N(1)-C(1)-S(1)	121.2(2)		
N(1)-C(1)-S(2)	115.9(2)	S(1)-C(1)-S(2)	122.89(18)		

Figure – 1

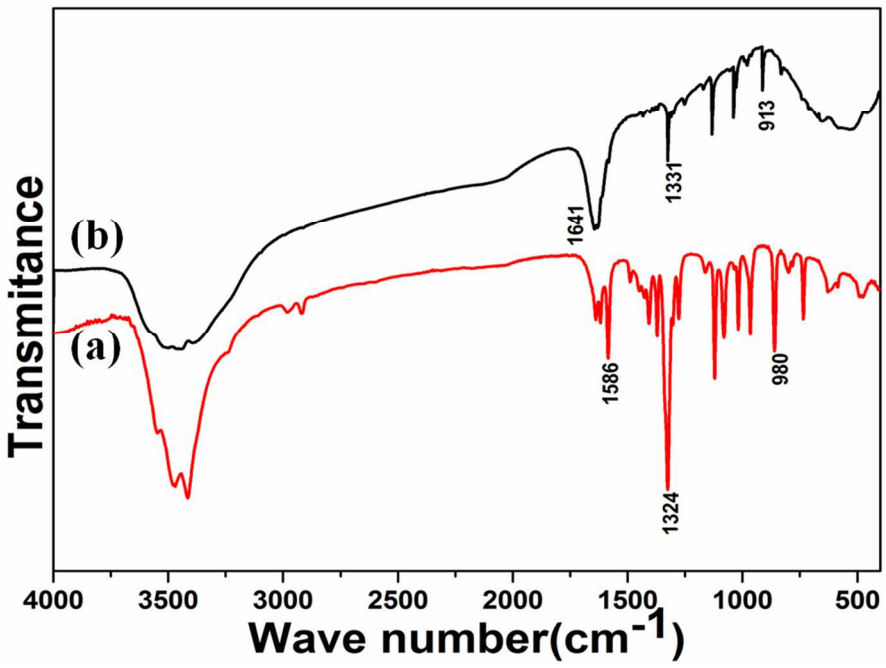

Figure - 2

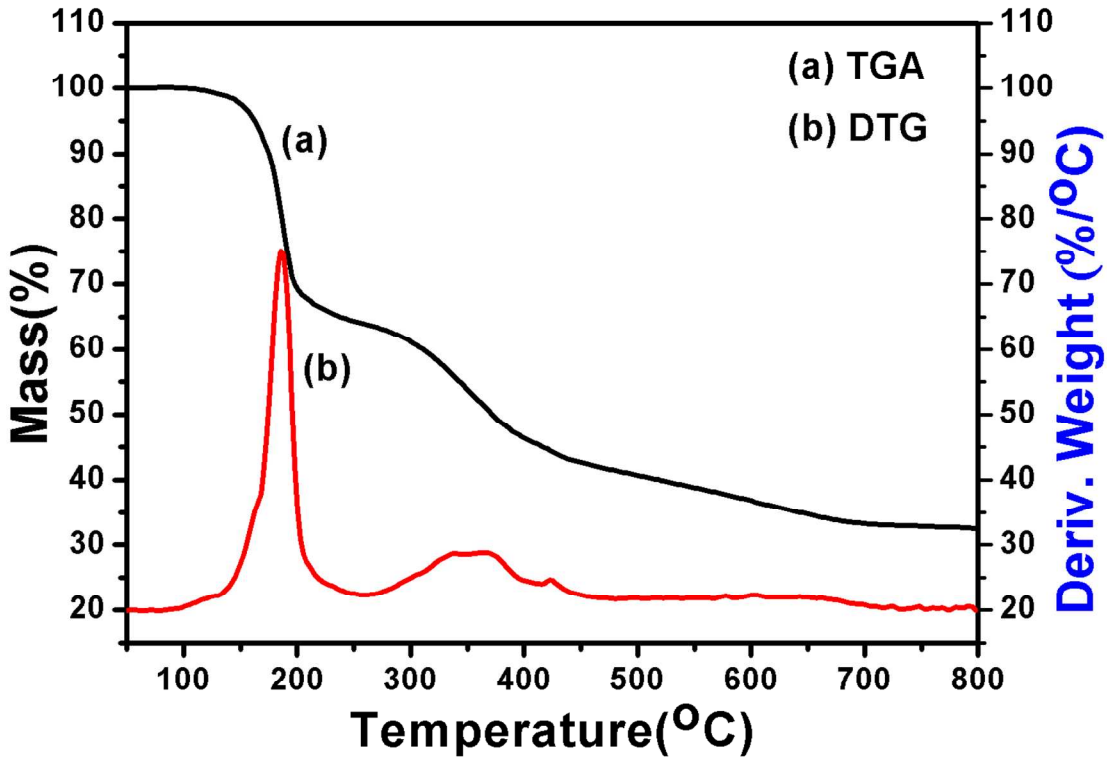

Figure – 3

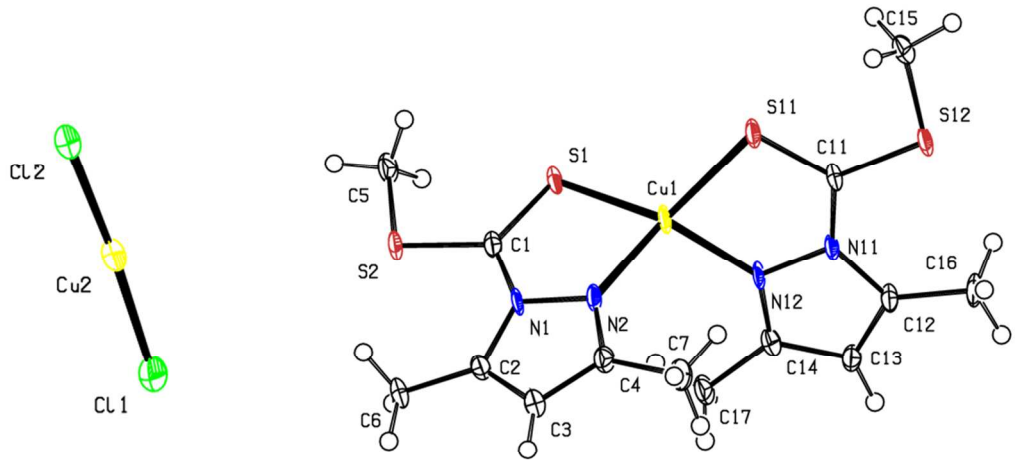

Figure – 4

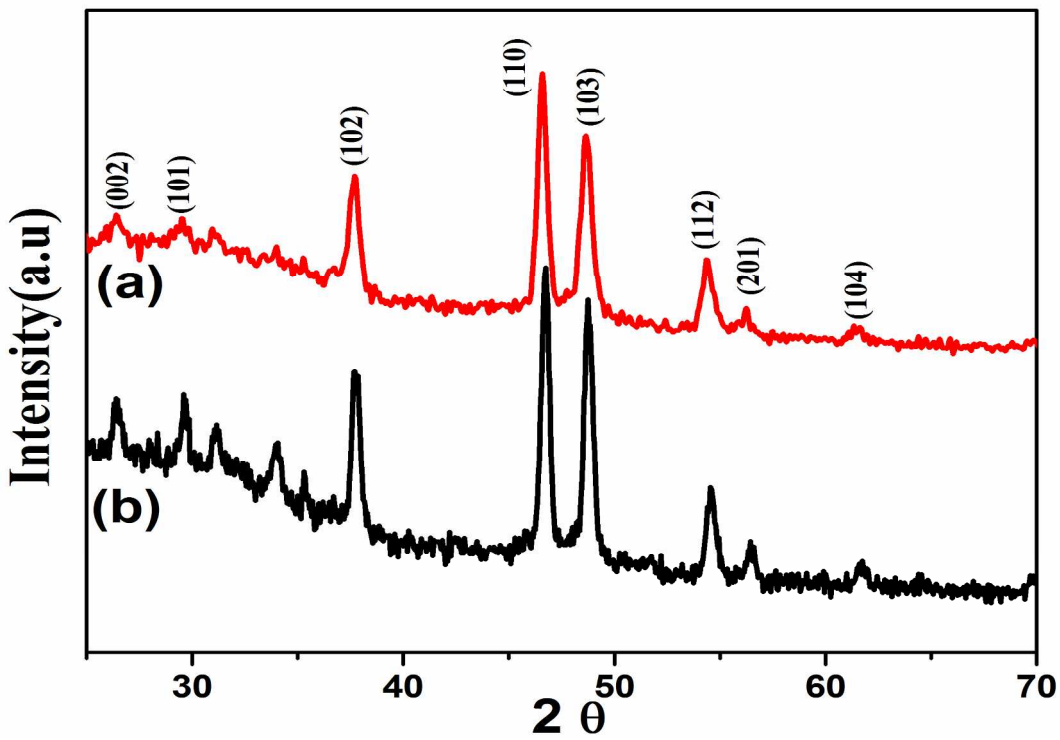

Figure – 5

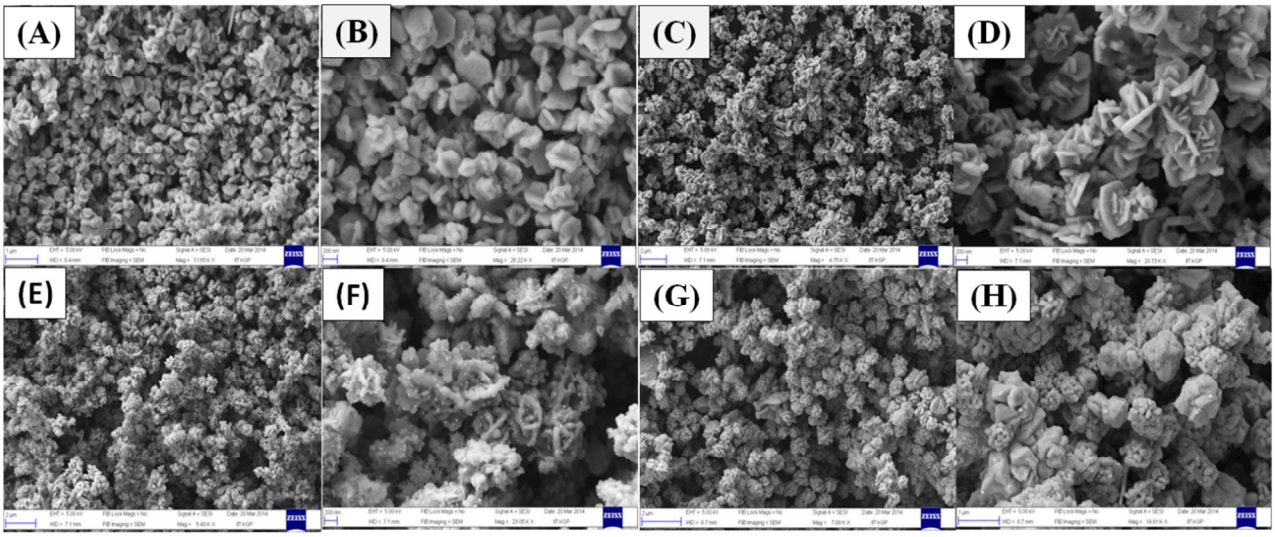

Figure – 6

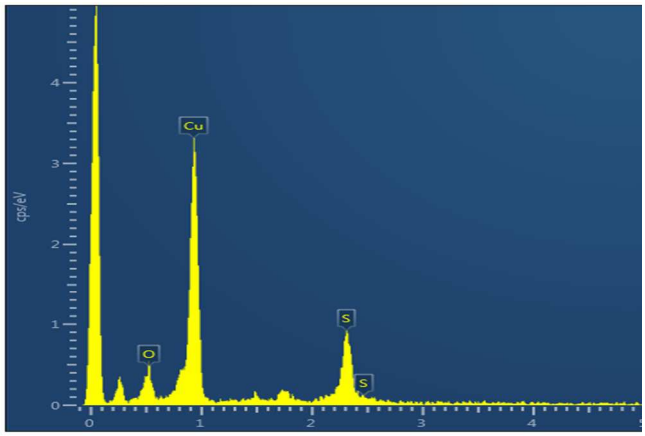

Figure – 7

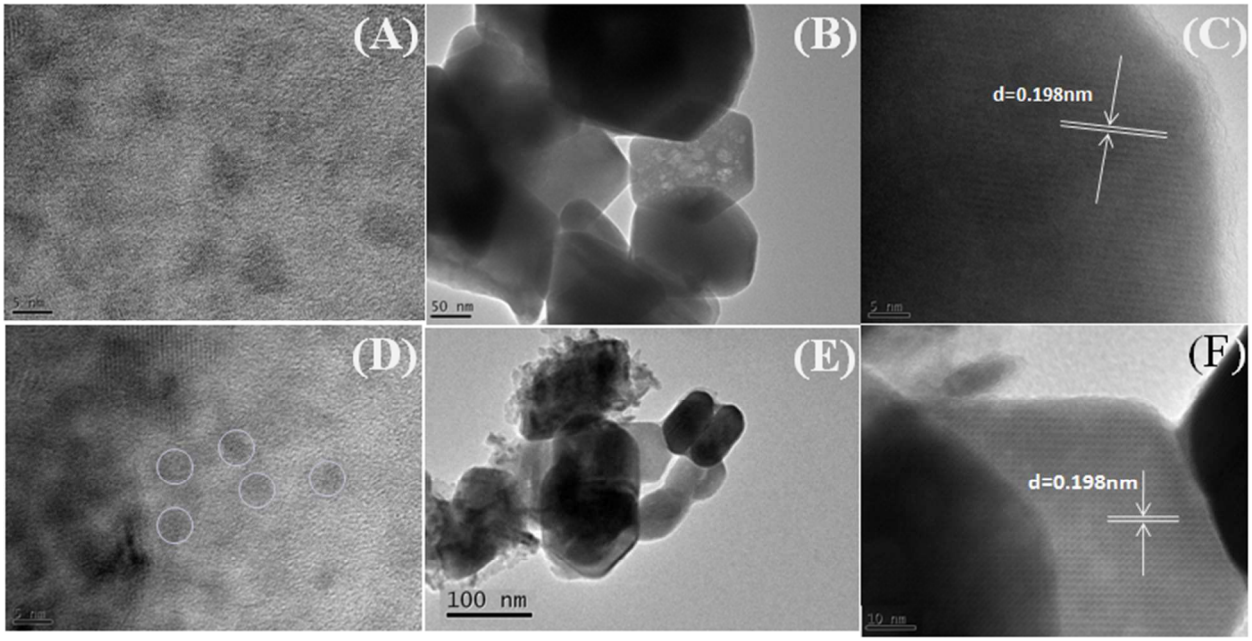

Figure – 8

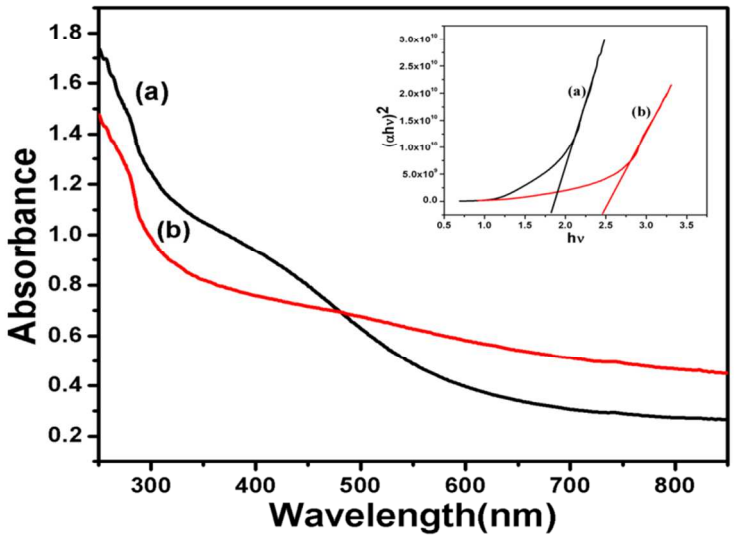

Figure – 9

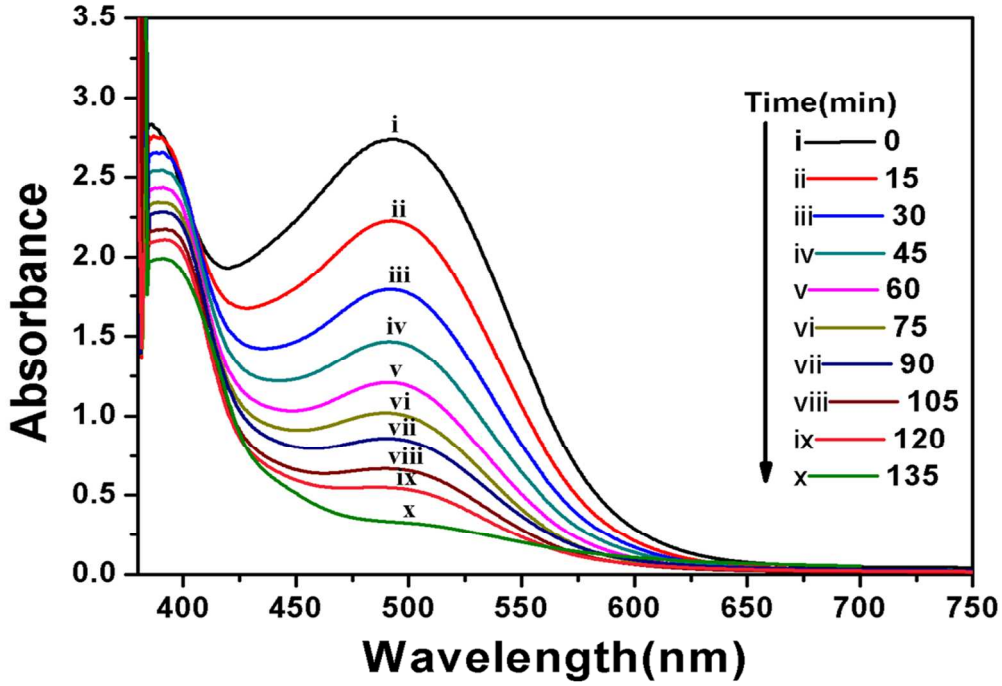

Figure – 10